Applied Catalysis B: Environmental 235 (2018) 56–65

Contents lists available at ScienceDirect

Applied Catalysis B: Environmental

journal homepage: www.elsevier.com/locate/apcatb

Fabrication of underpotentially deposited Cu monolayer/electrochemically reduced graphene oxide layered nanocomposites for enhanced ethanol electro-oxidation

Tuba Öznülüer[a], Ümit Demir[a], Hülya Öztürk Doğan[a,b,*]

[a] Department of Chemistry, Faculty of Sciences, Atatürk University, Erzurum, 25240, Turkey
[b] Department of Chemistry and Chemical Processing Technologies, Erzurum Vocational College, Atatürk University, Erzurum, 25240, Turkey

ARTICLE INFO

Keywords:
Electrochemical reduced graphene oxide
Nanocomposite
Electrochemical oxidation of ethanol
Electrocatalysis

ABSTRACT

Cu monolayer/electrochemically reduced graphene oxide (ML/ERGO) layered nanocomposites are grown on Au substrates by sequential underpotential deposition of Cu(ML)s and electrochemical reduction of graphene oxide for the electrocatalytic oxidation of ethanol. Characterization of the Au-Cu(ML)/ERGO layered composites by scanning electron microscopy and scanning tunneling microscopy reveal that the smooth Cu(ML) on the Au surface is transformed into parallel aligned nanoparticles after modification by the ERGO layer. X-ray photoelectron spectroscopy and Raman spectroscopy results for the Au-Cu(ML)/ERGO composites show the successful electrochemical reduction of GO to ERGO and the presence of metallic Cu in the nanocomposite structure. Electrochemical measurements of the as-prepared Au-(Cu(ML)/ERGO)$_1$ electrodes exhibit excellent electrocatalytic performance (15 mA cm^{-2}), which was 5.7 and 1.6 times higher than those from the naked Au and Au-Cu(ML) electrodes, respectively, toward ethanol electro-oxidation in alkaline condition.

1. Introduction

On account of the increasing demand for energy, new, environment friendly, renewable energy sources are now required. In particular, catalytic oxidation reactions of alcohols (methanol, ethanol, etc.) are becoming industrially more important because of their high energy efficiency, low operation temperatures, high power density, and low toxicity toward the environment [1–5]. Efficient and sustainable electrocatalysts for catalytic electro-oxidation of ethanol continue to be a topic of great research interest [6,7]. Pt and Pd are generally used as electrocatalysts for ethanol oxidation [8,9]. However, noble metallic electrodes such as Pd and Pt show a loss of activity due to reactive intermediates [10]. To improve the electrocatalytic activity of these metals, electrocatalysts structures such as nanoparticles, nanoflowers, nanotubes, nanodendrites, monolayer metal films, or ultra-thin composite layers have been investigated for electro-oxidation of ethanol [11,12]. In particular, metal monolayer-modified electrodes exhibit higher electrocatalytic activities toward electro-oxidation of ethanol than bulk metal electrodes [13,14]. Ultra-thin films can be easily synthesized by electrodeposition and the properties of the thin layer can be easily controlled by their size, crystallinity, shape and composition. Metal monolayers of Pt, Pd, Pb, Bi, Ag, Zn, and Cu on Au(111) electrodes have been reported to exhibit a remarkably high electrocatalytic activity toward hydrogen evolution reactions (HERs) and oxygen reduction reactions (ORRs) [10].

Au is considered to be an effective electrocatalyst toward ethanol oxidation in alkaline media [15]. However, the surface of Au is partially covered by Au oxides during ethanol oxidation reactions, and the reactivity of Au is decreased by the formation of strongly adsorbed oxygen species. For this reason, Au surface modification is important to prevent or reduce the adsorption of oxygen species. One of the methods of modification is underpotential deposition (UPD), which is used to form metal monolayers on the surfaces [16,17] or to synthesize a compound by depositing each element from their separate solutions [18,19]. Monolayers deposited during UPD on a Au electrode surface offer unique properties as electrocatalysts [20]. The reactivity of Au modified by monolayers of various metals (such as Pt, Pd, and Cd) toward ethanol oxidation is reported to be much higher than that of the unmodified Au surfaces [21–23]. Additionally, nanostructured Cu and Cu-based materials show a dramatic increase in overall catalytic activity. In particular, nanostructured Cu has been used for the electroreduction of CO_2 [24] and as a non-enzymatic glucose sensor [25]. In addition, graphene (G) and reduced graphene oxide (rGO) are used to form nanocomposites because of their unique properties. The superior

* Corresponding author at: Department of Chemistry and Chemical Processing Technologies, Erzurum Vocational College, Atatürk University, Erzurum, 25240, Turkey.
E-mail addresses: tozkim@atauni.edu.tr (T. Öznülüer), udemir@atauni.edu.tr (Ü. Demir), hdogan@atauni.edu.tr (H. Öztürk Doğan).

https://doi.org/10.1016/j.apcatb.2018.04.065
Received 28 December 2017; Received in revised form 31 March 2018; Accepted 26 April 2018
Available online 30 April 2018
0926-3373/

electrical conductivity and charge mobility of graphene-based materials has attracted much attention in recent years [26] for various applications, including catalysis and electrocatalysis. Recently, graphene-based composite electrodes such as Au-rGO nano dendrites [27], Pd/Cu/G [28], PtPd/Nafion-G [29], Pd NPs/PVP-G [30], Ni_xPd_{100-x}/G [31], etc. showed high catalytic activity for ethanol oxidation in an alkaline medium. Thus, G- and rGO-based metal composites have been synthesized to improve the performance of electrocatalysis by exploiting the specific advantages of graphene [32]. As a result of the synergistic effects of graphene sheets and metal monolayers, these nanocomposites offer novel physicochemical properties and can consequently improve electrocatalytic performance.

In the present study, we modified a Au surface with nanocomposites containing a Cu monolayer (Cu(ML)) deposited by UPD and electrochemically reduced graphene oxide (ERGO) to increase the electrocatalytic performance of Au electrodes. Morphological and analytical characterization studies indicated that the surface of the Au electrode is covered by nanostructured Cu(ML) and ERGO. Au electrodes modified by one layer of Cu(ML)/ERGO displayed the highest electrocatalytic performance toward ethanol oxidation among the naked Au, Au-Cu (ML), Au-$(Cu(ML)/ERGO)_3$ and Au-$(Cu(ML)/ERGO)_5$.

2. Experimental

2.1. Electrochemistry

The electrochemical experiments were carried out under an N_2 atmosphere, at room temperature in a three-electrode-system with an Ag/AgCl/3.5 M KCl electrode as reference electrode and a platinum wire as counter electrode using a BAS 100 W electrochemical analyzer and GAMRY potentiostat system. Single crystal Au(111) and polycrystalline Au wire electrodes were used as working electrodes. The electrochemically active surface area (ECSA) of the naked Au electrode was evaluated from the charge associated with the reduction of gold oxide by integration, which is proportional to the real active surface area of the gold surface (about 390 $\mu C\,cm^{-2}$) [33]. In addition, ECSA of the Cu (ML)-Au electrode was estimated by integration of the cathodic current from cyclic voltammetry. The charge of a Cu monolayer is about $\sim 420\,\mu C\,cm^{-2}$ [34]. The catalytic activities of the nanocomposite modified Au electrodes for ethanol oxidation were studied by cyclic voltammetry (CV), chronoamperometry and electrochemical impedance spectrometry (EIS). The CV measurements were recorded in N_2-deoxygenated solution of 1 M C_2H_5OH/0.5 M NaOH between -0.8 and 0.4 V at a scan rate of 50 mVs^{-1}. Chronoamperometry tests were measured at 0.2 V for 1200 s. EIS was carried out between 0.01 and 100,000 Hz with an AC voltage amplitude of 5.0 mV.

2.2. Layered composite preparation

The $(Cu/ERGO)_n$ (n = 1–5) layered nanocomposites on Au electrode were fabricated by sequential electrodeposition of Cu monolayer (Cu (ML)) at the UPD region and electrochemical reduction of GO to ERGO at the potential of -600 mV. The fabrication process of the working electrode is depicted in Fig. S1, Supporting information. Cu(ML) was electrodeposited on the bare Au or the ERGO modified Au surfaces from an aqueous solution containing 1 mM $CuSO_4$ in 50 mM H_2SO_4. Electrochemical reduction of GO on Cu(ML) modified Au surface (Au-Cu(ML)) or the Au-$[Cu(ML)/ERGO/Cu(ML)]_n$ surfaces were carried out from a suspension containing 1 mg/mL GO in 0.1 M KNO_3. Chemicals used for the Au modification ($CuSO_4$ and GO) were purchased from Sigma-Aldrich and used without further purification.

2.3. Characterization

The morphological characterizations were performed by scanning tunneling microscopy (STM, Molecular Imaging Model PicoScan) and field emission scanning electron microscope (FE-SEM, FEI Quanta). For STM, Pt/Ir wires (90:10) were employed as tunneling tips. X-ray photoelectron spectroscopy (XPS, PHI 5000 VersaProbe) and Raman spectroscopy (Wltech alpha 300R micro Raman system) measurements were performed for the qualitative and quantitative analysis of Au-$(Cu(ML)/ERGO)_n$ nanocomposites.

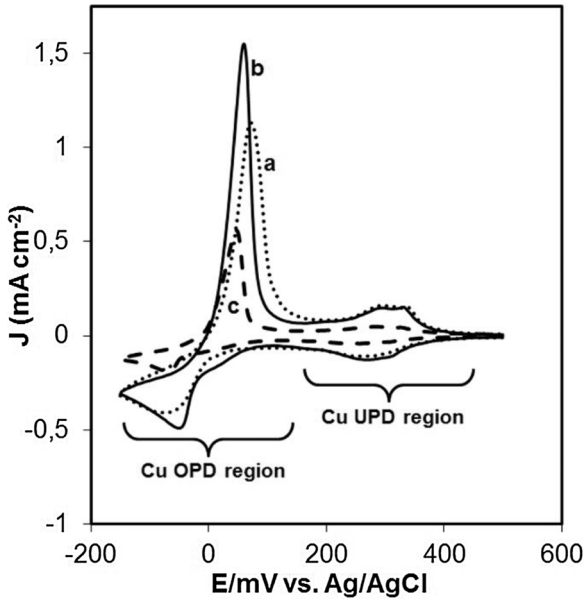

Fig. 1. Cyclic voltammograms of the naked Au **(a)**, Au-$(Cu(ML)/ERGO)_1$ **(b)**, and Au-$(Cu(ML)/ERGO)_3$ **(c)** electrodes in 50 mM H_2SO_4 solution containing 1 mM $CuSO_4$ at a scan rate 50 $mV\,s^{-1}$.

3. Results and discussion

3.1. Electrochemical layer-by-layer growth of $(Cu(ML)/ERGO)_n$

The electrochemical deposition technique used here was sequential electrochemical deposition of Cu monolayers by UPD and electrochemical reduction of GO to ERGO on the same Au electrode surface from two separate electrolyte solutions. Fig. 1(a) shows the cyclic voltammograms (CVs) for the UPD and overpotential deposition (OPD, bulk) of Cu on a polycrystalline Au electrode. The broad cathodic peak at -65 mV, which varies linearly with concentration and with the square root of the scan rate, is linear functions of concentration and the square root of the scan rate, is considered to denote the likely due to bulk deposition of Cu; meanwhile, the smaller cathodic peaks between 200 and 350 mV, correspond to surface-limited reactions and display a linear dependence on the square root of the scan rate, and correspond to surface-limited reactions, which can be attributed are ascribed to underpotential deposition (UPD) of Cu monolayers. A large anodic peak at 70 mV and small and broad peaks in the range of 240–380 mV correspond to the stripping of bulk Cu and UPD of Cu, respectively. These results are in good agreement with previously published results obtained for Cu electrodeposition on polycrystalline Au electrodes [35–37].

The electrodeposition of Cu at the UPD region immediately before reaching the electrodeposition potential for Cu OPD is shown to result in the formation of a Cu monolayer (Cu(ML)) [38,39]. Therefore, we first electrodeposited the Cu(ML) on the Au surface by setting up the deposition potential in the Cu UPD region. After electrodeposition of one Cu(ML) on an Au electrode to form a Cu(ML)-modified Au surface, we transferred the Cu(ML)-modified Au electrode into an electrolyte solution containing GO for the electrochemical reduction of GO to ERGO on the Au-Cu(ML) electrode. Fig. 2(a) shows the CVs recorded for the direct reduction of GO on an unmodified Au electrode indicating an

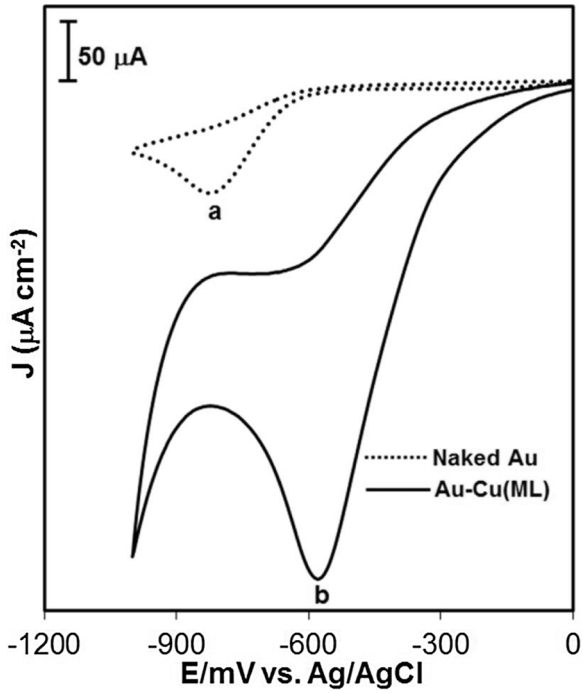

Fig. 2. Cyclic voltammograms for the electrochemical reduction of GO to ERGO on the naked Au **(a)** and on the Au-Cu(ML) **(b)** electrodes in an aqueous GO suspension. $\upsilon = 100\ mV\ s^{-1}$.

irreversible broad reduction curve in the range from −750 to −950 mV. It has been shown that this broad cathodic peak corresponds to the reduction of oxygen-bearing functional groups on GO [40–44]. The reduction potential should be lower than −900 mV for the nearly complete removal of oxygenated functional groups.

Fig. 2(b) shows the CVs for GO reduction after the modification of the same Au electrode by Cu(ML) under the same electrochemical conditions. As seen from the CVs, the reduction potential of GO shifted to more positive potential and the peak current density dramatically increased compared with the unmodified Au electrodes, meaning that the UPD-modified Au electrodes are more catalytically active and the kinetics of GO reduction are favorable. To determine whether this catalytic enhancement is because of the Cu metal or the Cu(ML)-modified Au electrode, we performed the same electrochemical reduction processes on pure Cu metal wire under the same electrochemical conditions. Fig. 3 shows linear sweep voltammograms for electrochemical reduction of GO on naked Au, naked metallic Cu wire, and the Cu(ML)-modified Au electrode.

As seen in Fig. 3, the electrochemical reduction of GO on the naked Cu wire has the lowest reduction potential and the smallest current density among the tested electrodes. The highest positive potential for the reduction of GO was observed using the Cu(ML)-modified electrode. Moreover, the steady-state peak current density for GO reduction on the Au-Cu(ML) electrode is much higher than that on the naked Au and Cu wire electrodes. These results clearly show that modification of the Au electrode with the Cu(ML) has a decisive effect on both the positive shift of the reduction potential, which means a lower overpotential is required to reduce GO compared with the naked Au, and the enhancement of the electrocatalytic effect of the Au-Cu(ML) electrode toward GO electroreduction. Electrochemical reduction of GO on Cu (ML)-Au could be a cost-effective, scalable, green route for producing high-quality ERGO with tunable carbon-to-cxygen (C/O) ratios. These results indicate that one layer of the Cu(ML)/ERGO composite structure could be fabricated on the surface of a Au electrode by sequential electrodeposition of Cu(ML) at the UPD region followed by electroreduction of GO at −600 mV for a short time.

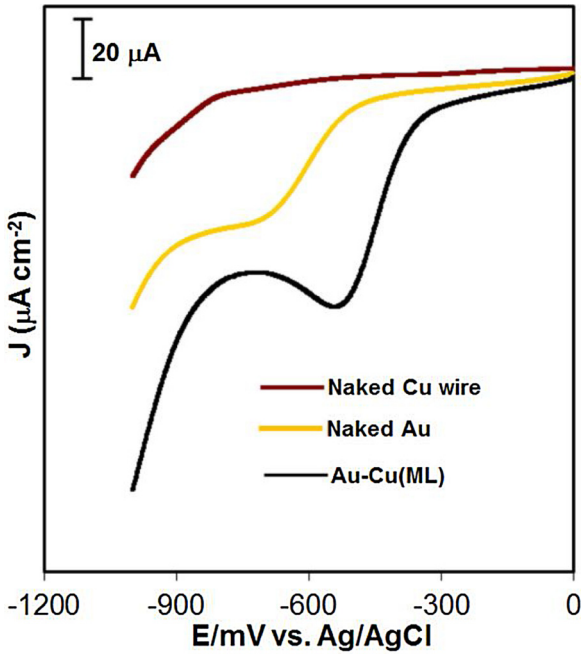

Fig. 3. Linear sweep voltammograms for electrochemical reduction of GO on naked Au, metallic Cu wire, and Cu(ML)-modified Au electrode.

To grow the second layer of the Cu(ML)/ERGO composite on top of the first layer of Cu(ML)/ERGO, we repeated the same sequential electrodeposition of Cu and ERGO on the top of Au-(Cu(ML)/ERGO)$_1$. UPD behavior is known to be defined by the naked metal surfaces [18]. Since the surface of the Au electrode changes after modification by one layer of the Cu(ML)/ERGO composite, electrodeposition by UPD may not be able to form additional Cu(ML)s on the Cu(ML)/ERGO-modified Au surface. To test this idea, we recorded the CV for Cu electrodeposition on the Au-(Cu(ML)/ERGO)$_1$ surface. The corresponding CV (Fig. 1(b)) for the electrodeposition of Cu on top of Au-(Cu(ML)-ERGO)$_1$ at the UPD region is similar to the one obtained for the naked Au, but the bulk deposition peak potential (E_{bulk}) shifted slightly to a less positive potential and the peak current increased, indicating that the surface-limited electrodeposition of Cu at the UPD region is not effected by the single layer of the Cu(ML)/ERGO composite. Therefore, the second layer of Cu could also be deposited on top of Au-(Cu(ML)/ERGO)$_1$ at the UPD region. Fig. 1(c) shows the CV recorded for Cu electrodeposition on top of the Au-(Cu(ML)/ERGO)$_3$ composite. As seen from Fig. 1(c), the peak currents at the UPD and OPD regions dramatically decreased and the shapes of the peaks were not similar to the ones obtained for the naked Au electrode. These results indicate that the modification of Au by Cu UPD is not valid for the fabrication of layered Cu(ML)/ERGO nanocomposites with more than 3 layers via the layer-by-layer growth technique described here.

3.2. Characterization of Cu(ML)/ERGO nanocomposites

The morphology and microstructures of the composites were investigated by FE-SEM and STM analysis. FE-SEM images of naked Au and Cu monolayer modified Au-Cu(ML) electrodes show a very smooth surface morphology with no irregularities, indicating no significant morphological change after Cu UPD (Fig. 4a).

Since STM enables the acquisition of high-resolution images of the electrode surface at an atomic scale, we recorded STM images of the Cu (ML)-modified Au(111) surface. As shown in Fig. 4(b), the Au(111) surface was covered by an adlayer of Cu(ML), which agrees with STM images recorded for Cu monolayers on Au(111) before [45–48]. Fig. 4(c) shows FE-SEM images of the Cu(ML)-modified electrode

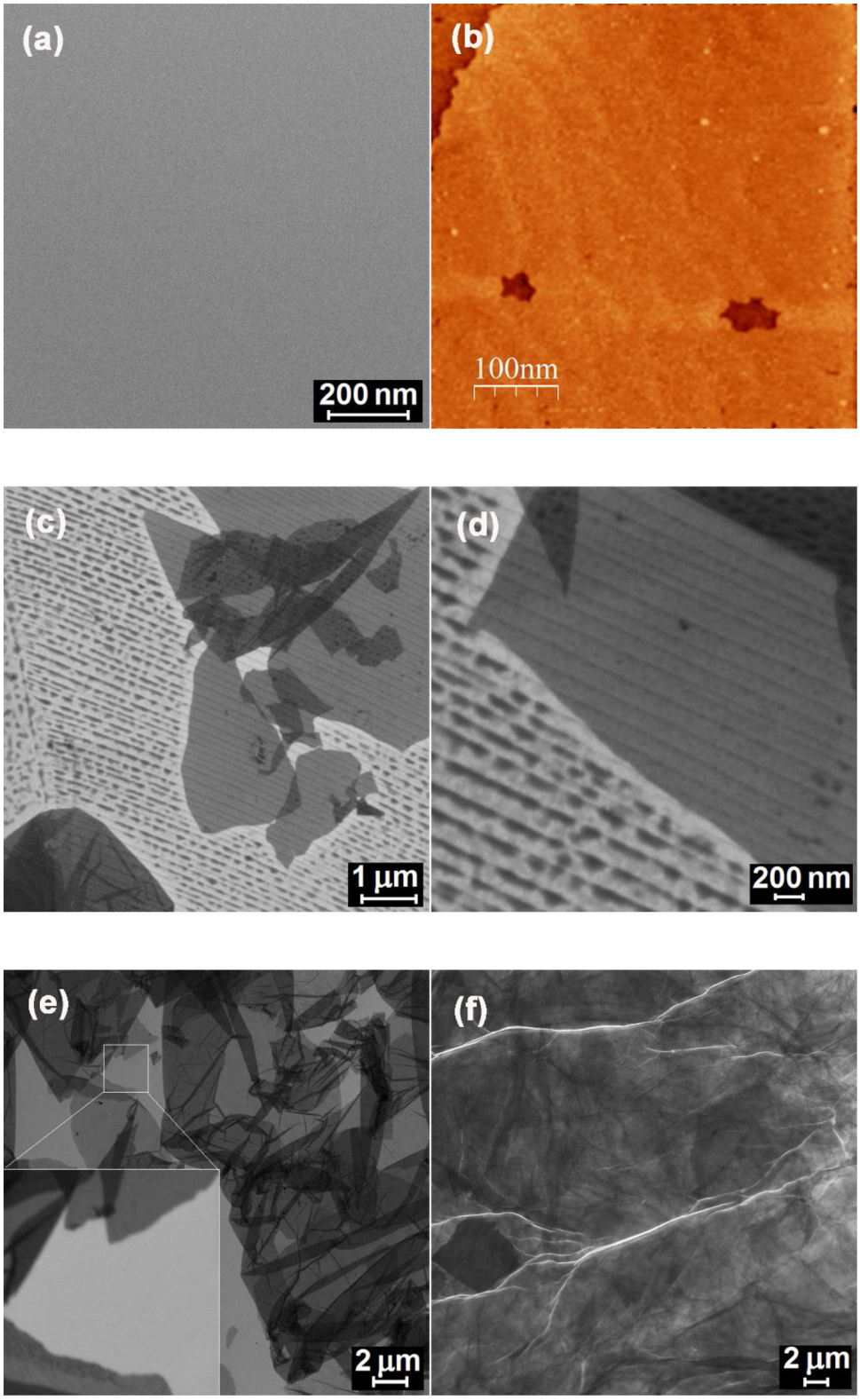

Fig. 4. FE-SEM **(a)** and STM **(b)** images of the Cu(ML)-modified Au(111) surface. FE-SEM images of Au-(Cu(ML)/ERGO)$_1$ **(c, d)**, Au-(Cu(ML)/ERGO)$_3$ **(e)**, and Au-(Cu(ML)/ERGO)$_5$ **(f)** nanocomposite electrodes.

surface after the electrochemical reduction of GO to ERGO at −600 mV for 1 min.

The surface morphology of Au-Cu(ML)/ERGO composites exhibited typical wrinkled and crumpled ERGO structures. The high-magnification FE-SEM (Fig. 4(d)) image revealed that the smooth Cu(ML) on the Au surface transformed into parallel aligned nanoparticles on both the Au surface and under the ERGO structures after modification by the ERGO layer. FE-SEM images of Au-(Cu(ML)/ERGO)$_3$ prepared by sequential electrodeposition of Cu and ERGO are shown in Fig. 4(e). This image and the inset clearly show that the surface morphology of Au-(Cu(ML)/ERGO)$_3$ is similar to that of Au-Cu(ML)/ERGO, except that the deposited Cu layers do not have a nanostructured morphology. The FE-

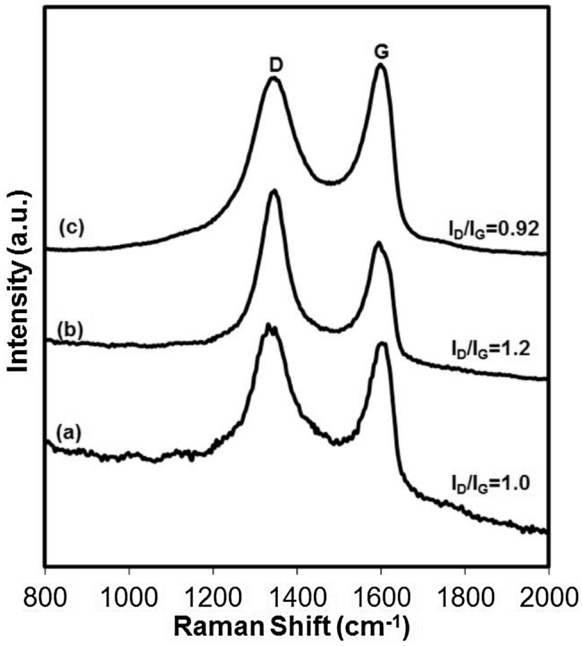

Fig. 5. Raman spectra of Au-GO **(a)**, Au-ERGO **(b)**, and Au-Cu(ML)/ERGO composite **(c)**.

SEM image shown in Fig. 4(f), obtained for Au-(Cu(ML)/ERGO)$_5$, indicated that the electrode surface was completely covered by the ERGO layers.

The Au-(Cu(ML)/ERGO)$_n$ composites were also investigated by Raman spectroscopy to determine the electroreduction performance of oxygen-bearing functional groups, as shown in Fig. 5. Two characteristic bands, the D and G bands, were observed in the Raman spectrum of the as-purchased GO, ERGO, and Cu(ML)/ERGO composite on the Au electrode. No other peaks related to Cu_xO species were observed in the Raman spectrum of Cu/ERGO, which indicated that the deposited Cu layer in the composite was metallic [49–51]. The G peaks at approximately 1600 cm^{-1} for Au-GO, 1595 cm^{-1} for Au-ERGO, and 1599 cm^{-1} for Au-Cu(ML)/ERGO are a result of the first-order scattering of the E_{2g} phonon of sp^2 C atoms [52,53]. The intensity ratios of the D band to the G band (I_D/I_G) for Au-GO, Au-ERGO and Au-Cu(ML)/ERGO were 1.0, 1.26, and 0.92 respectively. The increase in the I_D/I_G ratios from Au-GO to Au-ERGO can be attributed to the removal of oxygen functionalities from the surface of GO, indicating the successful electrochemical reduction of GO to ERGO, and an increase in defect concentration [54,55]. The I_D/I_G ratio decreased from 1.26 for Au-ERGO to 0.92 for Au-Cu(ML)/ERGO with sharp bands at 1355 and 1599 cm^{-1}, respectively. This behavior has been observed for bimetallic growth on ERGO and can be attributed to an increase in the sp^2 domain characteristics [56]. We believe that the Cu adlayers is more effective for the reduction of GO to ERGO because the interaction between Cu adlayers and the ERGO surface repairs the damaged sp^2 bonding network of ERGO or Cu adatoms in the Cu(ML)/ERGO composite are included in the ERGO structure.

The chemical states of the elements in the Cu(ML)/ERGO composites were examined by XPS measurements, as shown in Fig. 6. The XPS spectrum revealed the presence of Cu, O, and C without other elements in the composite. The binding energies observed at 932.2 and 951.9 eV were assigned to Cu2p$_{3/2}$ and Cu2p$_{1/2}$, which is consistent with the reported data for Cu 2p$_{3/2}$ binding energy values on metallic Cu (Fig.6(b)) [57,58]. Notably, the satellite peaks corresponding to Cu_xO species were not detected. Fig. 6(c) shows the C1s XPS spectra of the Cu/ERGO. For comparison, the XPS spectra of GO (as-purchased) is also shown in the same spectrum. The peaks can be fitted as three peaks at binding energies of at 284.9, 286.0, and 288.5 eV, which can be

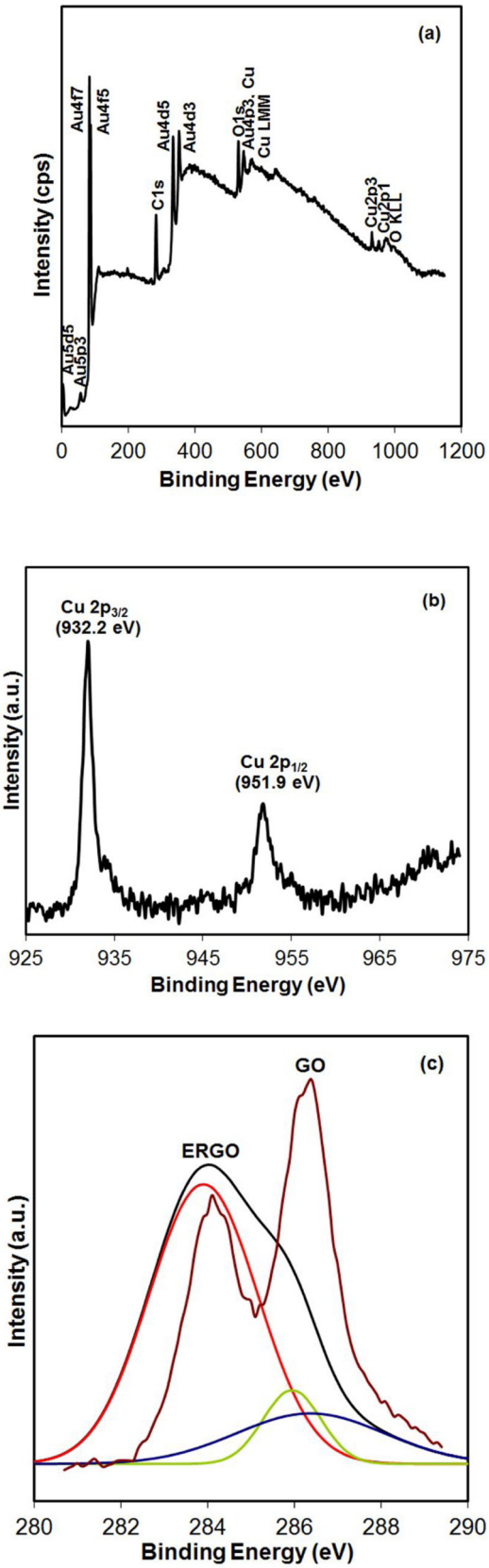

Fig. 6. XPS spectra: **(a)** survey spectrum **(b)** Cu 2p, and **(c)** C 1s of layered Cu (ML)/ERGO nanocomposites.

assigned to C—C, C—O—C, and O═C—O species, respectively. The intensities of the C—O and C═O peaks in the Cu(ML)/ERGO composite were much weaker than those in the GO used as a precursor, indicating that most chemically attached functional groups were successfully removed during the electrochemical reduction. By analyzing the C1 peak, values of 78.63% and 62.5% for the C—O—C and O═C—O species, respectively, are used to calculate the reduction ratio amount of different oxygen functional groups bonded with carbon. The intensity of peaks assigned to oxygen-containing functional groups of GO decreased significantly after electrochemical reduction.

These results indicate that the electrochemical reduction of GO to ERGO on Cu(ML) is so simple and efficient that it could not only be used for the electrosynthesis of ERGO-based nanocomposites but it could also be used for large-scale ERGO production for other applications.

3.3. Ethanol electro-oxidation on Au, Au-Cu(ML), and Au-(Cu(ML)/ERGO)$_n$ electrodes

The electrocatalytic activity of the Au-(Cu(ML)/ERGO)$_n$ nanocomposite electrodes for ethanol oxidation in alkaline media was studied using CVs. The CVs of bare Au, Au-Cu(ML), and Au-Cu(ML)/ERGO electrodes in 0.5 M NaOH solution containing 1 M ethanol are displayed in Fig. 7. The CVs shown in Fig. 7 exhibit a prominent anodic peak located at approximately 0.2 V in the anodic (forward) scan for all electrodes, and this peak can be attributed to ethanol electro-oxidation at the bare polycrystalline Au electrode. In the cathodic (backward) scan, another anodic peak at approximately 0.1 is clearly seen, and this peak corresponds to the removal of incompletely oxidized and adsorbed CO-like carbonaceous species formed in the forward scan. These observations are in good agreement with previous studies performed on the electro-oxidation of ethanol on Au electrodes [23,59,60]. However, Pandey et al. reported that the reverse anodic peak behavior can be explained by the high energy sites formed after the reduction of the blocking gold oxide film [60,61]. Some crystalline surfaces of Au have higher electrocatalytic activity for ethanol oxidation in alkaline media than the other metal electrodes such as Pt and Pd [62]. Fig. 7(b) shows the CVs obtained for electro-oxidation of ethanol after Cu UPD on the same Au electrode under the same electrochemical conditions. All of the CV curves are typical features of ethanol electro-oxidation in basic media, but the anodic peak current density increased and the anodic peak potentials shifted to less positive potentials, indicating the enhanced electrocatalytic activity of the Au-Cu(ML) electrode compared with the naked Au electrode. The CVs shown in Fig. 7(c) were recorded for the electro-oxidation of ethanol on Au-(Cu(ML)/ERGO) prepared by the reduction of GO on the Au-Cu(ML) electrode. The CVs for the Au-Cu(ML)/ERGO electrodes in the presence and absence of ethanol are also presented in the same figure for comparison. The anodic peak potential of electrochemical oxidation of ethanol on the Au-Cu(ML)/ERGO electrode is 200 mV, approximately and ~ 20 mV more negative than that on the Au-Cu(ML) electrode. Electrochemical parameters obtained from CVs and Tafel slopes at the different catalyst-coated electrodes in a solution of 0.5 M NaOH and 1 M ethanol is given Table 1. These results indicate that the Au-Cu(ML)/ERGO nanocomposite electrode exhibited much better electrocatalytic activity than the naked Au and Cu(ML)-Au electrodes. The catalyst tolerance to intermediate carbonaceous species is often evaluated using the ratio of the forward anodic peak current (I_f) to the backward anodic peak current (I_b). The I_f/I_b value for Au-Cu(ML)/ERGO is 2.66, which is lower than those for electrochemical oxidation of ethanol on Pd or Pt-based electrocatalysts [63,64], indicating the improved performance with respect to removal of incompletely oxidized carbon species via oxidation in the reverse scan from the surface. The high oxidation activity for some of the alcohols in alkaline media on Au compared with Pt could be related to the high resistance of Au toward the formation of poisoning surface oxides [62].

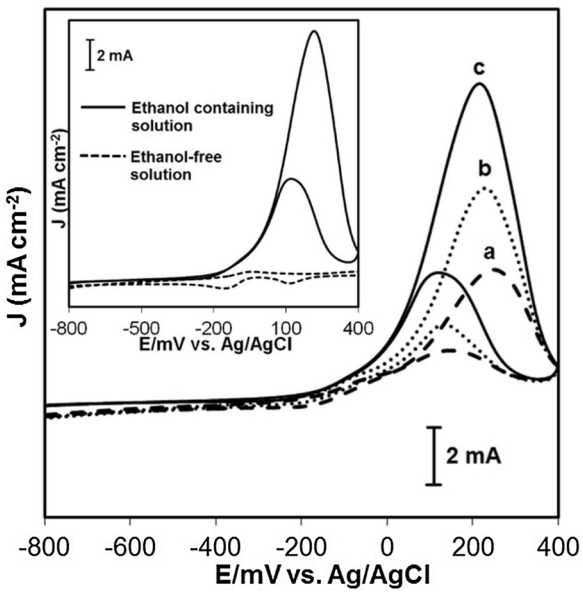

Fig. 7. Cyclic voltammograms of the naked Au **(a)**, Au-Cu(ML) **(b)**, and Au-Cu (ML)/ERGO **(c)** electrodes in 1 M C_2H_5OH/0.5 M NaOH electrolyte.

Table 2 lists the peak potential and peak current density for electro-oxidation of ethanol on different electrocatalysts. The peak current density for ethanol oxidation on Au-(Cu(ML)/ERGO)$_1$ has been found to be 15 mA cm^{-2}, which was about 2–60 times higher than those observed for different electrodes. And also the as-prepared Au-(Cu(ML)/ERGO)$_1$ electrodes exhibited 5.7 and 1.6 times higher current density than those from the naked Au and Au-Cu(ML) electrodes, respectively, under alkaline conditions. The higher peak current density indicates that ethanol has a higher conversion efficiency for the ethanol electro-oxidation on Au-(Cu(ML)/ERGO)$_1$ electrode [65]. In addition, the onset potential of the forward anodic peak of the Au-(Cu(ML)/ERGO)$_1$ electrode is obviously lower than those of the Au-Cu(ML) and naked Au electrodes, indicating it is much more favorable for ethanol electro-oxidation (Table 1) [66].

Fig. 8 shows Tafel plots of ethanol electro-oxidation on naked Au, Au-Cu(ML) and Au-(Cu(ML)/ERGO)$_1$ electrodes and calculations of the Tafel slopes yielded the values 122, 91.5, and 77.6 mV dec^{-1}, respectively, in the linear region between −0.08 to −0.135 V. As summarized in Table 1, Tafel slope values decrease with the addition of either Cu (ML) or (Cu(ML)/ERGO)$_1$ to Au; the number of electrons transferred also increase. The Tafel slope value obtained for the Au catalyst, 122 mV dec^{-1}, can be attributed to ethanol electro-oxidation as controlled by the adsorption of OH_{ads}. Lower Tafel slope values were obtained with the addition of either Cu(ML) or (Cu(ML)/ERGO)$_1$, which indicate that these catalysts exhibit faster ethanol electro-oxidation charge-transfer kinetics. The fastest kinetics were observed for the Au-(Cu(ML)/ERGO)$_1$ electrode due to synergy between Cu and ERGO. Strong interaction of Cu and ERGO with the electrolyte forms oxygenated intermediates which results in faster charge-transfer kinetics and enhanced ethanol electro-oxidation.

Complete oxidation of ethanol is a complex 12-electron transfer reaction. Using FTIR, Bianchini [71] and Zhou [72] showed that the ability of Pd to break the C—C bond of ethanol was slightly better than that of Pt under the same conditions; however, the overall selectivity for ethanol oxidation to CO_2 was still low, around 2.5%. The products of the ethanol electro-oxidation on Au-(Cu(ML)/ERGO)$_1$ electrode were investigated by cyclic voltammetry in 0.5 M NaOH solutions containing ethanol, acetaldehyde, and sodium acetate. Fig. 9 shows that although the electro-oxidation of acetaldehyde has similar features compared to that of ethanol, it has a slightly higher current density and a peak potential with a significant positive shift. On the other hand, no distinct oxidation current is observed in the sodium acetate solution. Similar

Table 1
Electrochemical parameters obtained from CVs and Tafel slopes at the different electrodes in 0.5 M NaOH containing 1 M ethanol.

	Potential (mV)			Current Density (mA cm^{-2})				
Electrode	E_{onset}[a]	E_f[b]	E_b[c]	I_f[d]	I_b[e]	J_o[f]	αn[g]	Tafel slope (mV dec^{-1})
Au	−725	+251	+145	2.71	0.97	0.1128	0.48	122
Au-Cu(ML)	−732	+218	+137	9.38	3.48	0.38	0.64	91.5
Au-Cu(ML)/ERGO	−778	+195	+115	15.3	5.75	0.40	0.76	77.6

[a] Onset potential.
[b] Forward Peak Potential.
[c] Backward Peak Potential.
[d] Forward Peak Current Density.
[e] Backward Peak Current Density.
[f] Exchange current density.
[g] Transfer coefficient for ethanol electro-oxidation.

results have been obtained for the ethanol electro-oxidation on the Pd electrode [73].

The catalytic activity and stability of the Au-(Cu(ML)-ERGO) electrocatalyst were further investigated using the current density vs time (I vs. t) curves recorded in 1 M C_2H_5OH + 0.5 M NaOH solution at a potential of 200 mV (Fig. 10). An initially rapid current decay was found for all electrocatalysts because of the accumulation of poisonous carbonaceous intermediates generated during the ethanol electro-oxidation reaction. Subsequently, the current decreased slowly and reached steady state for all electrocatalysts. In particular, Au-Cu(ML)/ERGO catalyst exhibits a current density that is almost 9 times than that of the Au electrode after a reaction that lasted 3000 ms; this indicates that the electrocatalytic performance of the Au-Cu(ML)/ERGO nanocomposite electrode toward electrochemical oxidation of ethanol is stable. The current density for ethanol oxidation on the Au-Cu(ML)/ERGO electrode was 15 mA cm^{-2}, which is 5.7 and 1.6 times higher than that for the naked Au and Au-Cu(ML) electrode, respectively. This demonstrates that the Au-Cu(ML)/ERGO catalyst shows relatively rapid reaction kinetics.

Fig. 11 shows the catalytic activity of the Au-(Cu(ML)/ERGO)$_1$, Au-(Cu(ML)/ERGO)$_3$, and Au-(Cu(ML)/ERGO)$_5$ layered nanocomposites prepared by the sequential electrodeposition of Cu and ERGO with two and three layers of Cu(ML)/ERGO on the Au electrode. Interestingly, the Au electrode modified with a single layer of Cu(ML)/ERGO shows the highest efficiency for electro-oxidation of ethanol among these electrocatalysts. Fig. 11 indicates that the activity of the Au-Cu(ML)/ERGO electrode decreases as the number of Cu(ML)/ERGO layers increases.

To understand the increased activity of the single-layer Cu(ML)/ERGO composite compared with the other composites, the electrochemical impedance spectrum (EIS) of the Au-(Cu(ML)/ERGO)$_1$, Au-(Cu(ML)/ERGO)$_3$, and Au-(Cu(ML)/ERGO)$_5$ composite electrodes was measured at an electrode potential of 200 mV in a 1 M C_2H_5OH/0.5 M NaOH solution; the corresponding Nyquist plots are shown in Fig. 12. The measured impedance spectra of the electrodes were fitted using the complex nonlinear least square (CNLS) fitting method [74] and the equivalent circuit [75]. EIS is an important tool for the study of the characteristics of conductivity and charge transport at the material/electrolyte interface. The intersection of the curves in the real part

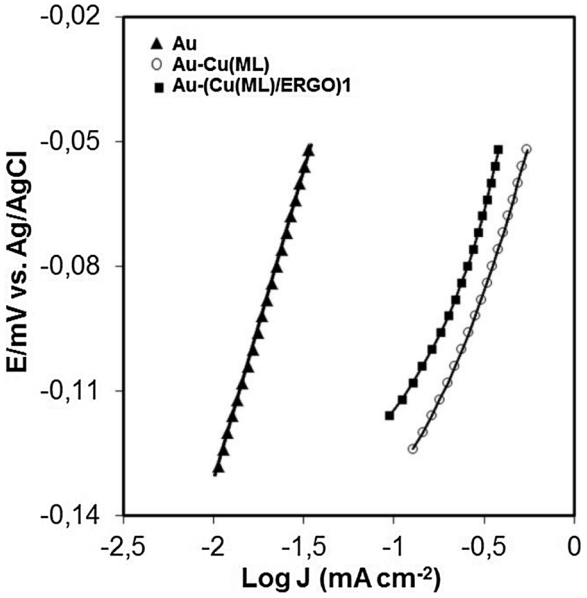

Fig. 8. Tafel plots of the Au, Au-Cu(ML) and Au-(Cu(ML)/ERGO) electrodes in 1 M ethanol containing 0,5 M NaOH electrolyte at 1 mV s^{-1} scan rate.

Table 2
Comparison of the peak potential, peak current density of different electrodes for the electro-oxidation of ethanol.

Electrode	Electrolyte	Ethanol Concentration (mol L^{-1})	E_f (V)[c]	I_f (mA cm^{-2})[d]	Ref.
Polycrystalline Au	0.1 M KOH	0.1	+1.15 (RHE)	0.5	[67]
Au-rGO	1.0 M KOH	1.0	−0.61 (Ag/AgCl)	2.3	[27]
Au/GO	0.1 M NaOH	1.0	+0.19 (SCE)	5.06	[68]
Pd-Au/rGO	1.0 M KOH	1.0	−0.054 (Hg/HgO)	0.98	[69]
$Pd_{0.50}Cu_{0.50}$/C	1.0 M NaOH	0.5	−0.27 (Hg/HgO)	0.25	[70]
Pd/Cu/G[a]	1.0 M KOH	1.0	−0.28 (SCE)	3.53	[28]
PtPd/Nafion-G	0.5 M NaOH	1.0	−0.2 (Ag/AgCl)	7.69	[29]
Pd NPs/PVP-G[b]	1.0 M NaOH	0.5	−0.1 (Ag/AgCl)	1.08	[30]
(Cu(ML)/ERGO)$_1$	0.5 M NaOH	1.0	0.2 (Ag/AgCl)	15	This work

[a] G; Graphene.
[b] PVP; Poly(Vinyl Pyrrolidone).
[c] Anodic peak potential.
[d] Current density of ethanol electro-oxidation.

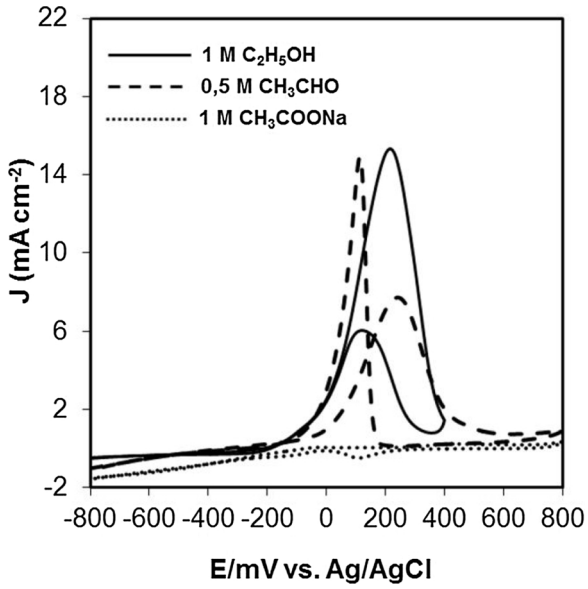

Fig. 9. Cyclic voltammograms of Au-(Cu(ML)/ERGO) electrode for the oxidation of acetaldehyde (CH_3CHO, 0.5 M), sodium acetate (CH_3COONa, 1 M), and ethanol (CH_3CH_2OH, 1 M) in 0.5 M NaOH solution.

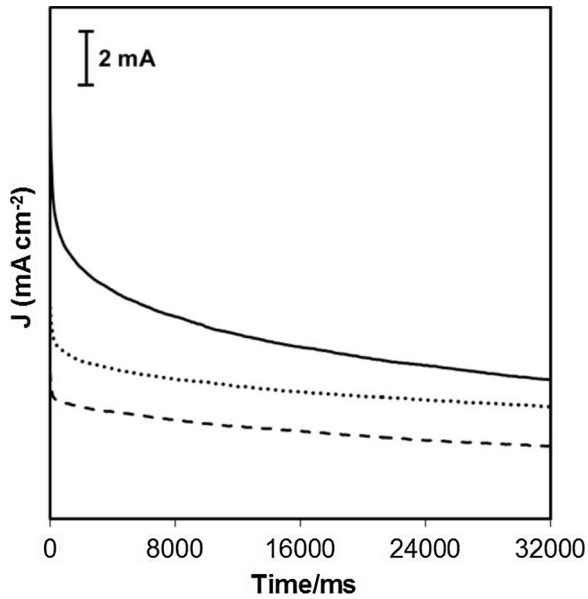

Fig. 10. Chronoamperograms for Au, Au-Cu(ML), and Cu(ML)/ERGO electrodes in 0.5 M NaOH solution containing 1 M C_2H_5OH.

represents the equivalent series resistance (ESR) of the electrochemical system and the semicircles display the charge-transfer process (R_{ct}) at the working electrode–electrolyte interface [76,77]. The estimated ESR values from Fig. 11 for Au-(Cu(ML)/ERGO)$_1$, Au-(Cu(ML)/ERGO)$_3$, and Au-(Cu(ML)/ERGO)$_5$ composite electrodes are all approximately 1.2 O, indicating that all the composite electrodes have the same high electrical conductivity. This behavior can be attributed to the increased contact between the Au electrode and the Cu(ML)/ERGO) composite material resulting from direct electrochemical reduction of the Cu adlayer and GO on the electrodes. However, the (R_{ct}) of the Au-(Cu(ML)/ERGO)$_1$, Au-(Cu(ML)/ERGO)$_3$, and Au-(Cu(ML)/ERGO)$_5$ composite electrodes estimated from the semicircles in the EIS spectra of the fabricated composites increase to 2, 6, and 21.5 kΩ with increasing number of Cu(ML)-ERGO layers deposited on the Au electrode. The small semicircle loops in the high-frequency region and low ESR values

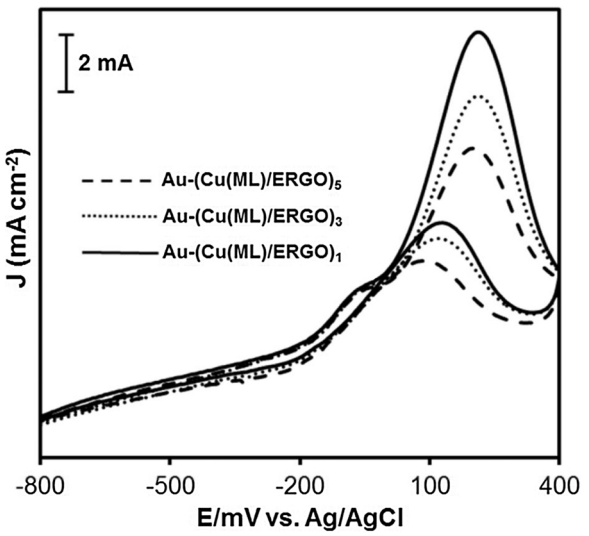

Fig. 11. CVs of Au-(Cu(ML)/ERGO)$_1$, Au-(Cu(ML)/ERGO)$_3$ and Au-(Cu(ML)/ERGO)$_5$ composites in 1 M C_2H_5OH/0.5 M NaOH electrolyte at a scan rate of 50 mV s^{-1}.

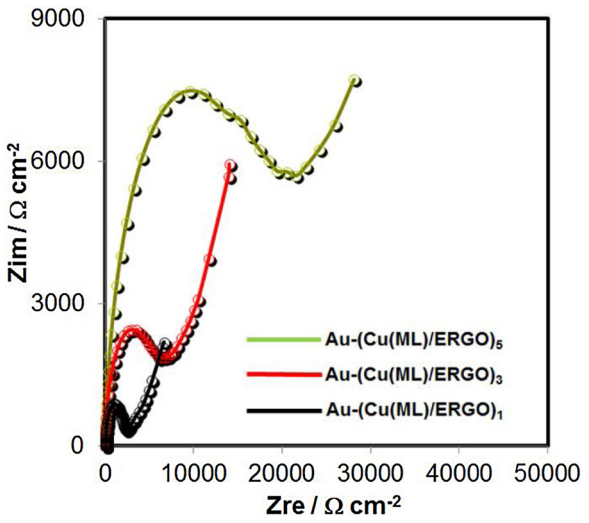

Fig. 12. EIS spectra of the Au-(Cu(ML)/ERGO)$_1$, Au-(Cu(ML)/ERGO)$_3$, and Au-(Cu(ML)/ERGO)$_5$ composite electrodes measured at an AC amplitude of 5 mV, in 1 M C_2H_5OH/0.5 M NaOH aqueous electrolyte.

for the Au-(Cu(ML)/ERGO)$_1$ indicate the lowest charge-transfer resistance and high electrical conductivity, which are beneficial for improving the performance of the electrocatalytic activity toward ethanol electro-oxidation. In addition, the steeper slope in the low-frequency region for the Au-(Cu(ML)/ERGO)$_1$ composite indicates fast ion transport in the composite electrode. All of these EIS results can help explain why the Au-(Cu(ML)/ERGO)$_1$ composite electrode had a higher catalytic activity for ethanol oxidation than the Au-(Cu(ML)/ERGO)$_3$ and Au-(Cu(ML)/ERGO)$_5$ electrodes.

On the basis of the FE-SEM, cyclic voltammetry, and EIS results, the improved catalytic performance toward ethanol oxidation of the Au-(Cu(ML)/ERGO)$_1$ composite electrode in alkaline media can be explained as follows. First, the single layer of the Cu(ML)/ERGO composite is so thin that it could not weaken the excellent catalytic activity of Au in alkaline media. Second, the Cu adlayers could play an important role in improving the catalytic activity of the electrode. The metal monolayers on various electrode materials deposited underpotentially were reported to exhibit a remarkably high electrocatalytic activity toward ORRs [78–80]. Third, the ERGO sheets with their particular properties

(e.g., large surface area and excellent charge conductivity) benefit the transfer of electrons. Fourth, as shown by the FE-SEM images of the Au-$(Cu(ML)/ERGO)_1$ composite, the Cu adlayers were converted into small nanostructured domains after electroreduction of GO, which enables the Cu nanostructures to have increased numbers of exposed active sites. These Cu/ERGO nanostructures may therefore have more interaction sites between ERGO and Cu adlayers, which can enhance the catalytic activity of the electrode. As a result of these multiple factors, the Au-$(Cu(ML)/ERGO)_1$ electrode shows a higher activity than the Au-$(Cu(ML)/ERGO)_3$ and Au-$(Cu(ML)/ERGO)_5$ composite electrodes.

4. Conclusions

We reported a simple and controllable electrochemical deposition method based on the sequential electrodeposition of Cu(ML) in the UPD region, followed by the electroreduction of GO to ERGO, for the fabrication of layered Au-$(Cu(ML)/ERGO)_n$ nanocomposite electrodes. We have demonstrated that Au electrodes modified by a single layer of Cu (ML)/ERGO nanocomposite have the highest electrocatalytic activity toward electrochemical oxidation of ethanol in alkaline solution. The current density for the ethanol electro-oxidation reaction on the Au-Cu (ML)/ERGO electrode is 15 mA cm^{-2}, which is 5.7 and 1.6 times higher than that for naked Au and Au-Cu(ML) electrodes, respectively. Interestingly, we found that the activity of the Au-Cu(ML)/ERGO electrode decreases as the number of Cu(ML)/ERGO layers increases. These results suggest that the Au-Cu(ML)/ERGO nanocomposite electrode can be used as an electrocatalyst for alkaline direct ethanol fuel cells.

Acknowledgements

The authors wish to thank the Scientific and Technological Research Council of Turkey (TÜBİTAK, Proj. No: 112T791), for the financial support of this work.

Appendix A. Supplementary data

Supplementary material related to this article can be found, in the online version, at doi:https://doi.org/10.1016/j.apcatb.2018.04.065.

References

[1] Y.J. Hu, H. Zhang, P. Wu, H. Zhang, B. Zhou, C.X. Cai, Bimetallic Pt-Au nanocatalysts electrochemically deposited on graphene and their electrocatalytic characteristics towards oxygen reduction and methanol oxidation, Phys. Chem. Chem. Phys. 13 (2011) 4083–4094.
[2] Q. Tan, C.Y. Du, Y.R. Sun, L. Du, G.P. Yin, Y.Z. Gao, Nickel-doped ceria nanoparticles for promoting catalytic activity of Pt/C for ethanol electrooxidation, J. Power Sources 263 (2014) 310–314.
[3] W.H. Yang, H.H. Wang, D.H. Chen, Z.Y. Zhou, S.G. Sun, Facile synthesis of a platinum-lead oxide nanocomposite catalyst with high activity and durability for ethanol electrooxidation, Phys. Chem. Chem. Phys. 14 (2012) 16424–16432.
[4] L.H. Yu, J.Y. Xi, TiO2 nanoparticles promoted Pt/C catalyst for ethanol electrooxidation, Electrochim. Acta 67 (2012) 166–171.
[5] M.Z.F. Kamarudin, S.K. Kamarudin, M.S. Masdar, W.R.W. Daud, Review: direct ethanol fuel cells, Int. J. Hydrogen Energy 38 (2013) 9438–9453.
[6] N.M. Julkapli, S. Bagheri, Graphene supported heterogeneous catalysts: an overview, Int. J. Hydrogen Energy 40 (2015) 948–979.
[7] L. Rao, Y.X. Jiang, B.W. Zhang, L.X. You, Z.H. Li, S.G. Sun, Electrocatalytic oxidation of ethanol, Prog. Chem. 26 (2014) 727–736.
[8] D.H. Nagaraju, S. Devaraj, P. Balaya, Palladium nanoparticles anchored on graphene nanosheets: methanol, ethanol oxidation reactions and their kinetic studies, Mater. Res. Bull. 60 (2014) 150–157.
[9] L. Wang, Q. Li, T. Zhan, Q. Xu, A review of Pd-based electrocatalyst for the ethanol oxidation reaction in alkaline medium, Adv. Mater. Res. Energy Dev. 860–863 (2014) 826–830.
[10] S. Kocak, Z. Dursun, F.N. Ertas, Electrocatalytic oxidation of methanol at Pd and Pt ad-layer modified Au(111) electrodes in alkaline solution, Turk. J. Chem. 35 (2011) 711–722.
[11] H. Begum, M.S. Ahmed, S. Jeon, Highly efficient dual active palladium nanonetwork electrocatalyst for ethanol oxidation and hydrogen evolution, ACS Appl. Mater. Interfaces 9 (2017) 39303–39311.
[12] M.T.M. Koper, Structure sensitivity and nanoscale effects in electrocatalysis, Nanoscale 3 (2011) 2054–2073.
[13] W.C. Liao, S. Yau, Au(111)-Supported Pt monolayer as the most active electrocatalyst toward hydrogen oxidation and evolution reactions in sulfuric acid, J. Phys. Chem. C 121 (2017) 19218–19225.
[14] C.Z. Zhu, S.F. Fu, Q.R. Shi, D. Du, Y.H. Lin, Single-atom electrocatalysts, Angew. Chem. Int. Ed. 56 (2017) 13944–13960.
[15] J.L. Gong, C.B. Mullins, Selective oxidation of ethanol to acetaldehyde on gold, J. Am. Chem. Soc. 130 (2008) 16458-+.
[16] A. Gichuhi, B.E. Boone, U. Demir, C. Shannon, Electrochemistry of S adlayers at underpotentially deposited Cd on Au(111): implications for the electrosynthesis of high-quality CdS thin films, J. Phys. Chem. B 102 (1998) 6499–6506.
[17] T. Oznuluer, U. Demir, Formation of Bi2S3 thin films on Au(111) by electrochemical atomic layer epitaxy: kinetics of structural changes in the initial monolayers, J. Electroanal. Chem. 529 (2002) 34–42.
[18] I.Y. Erdogan, T. Oznuluer, F. Bulbul, U. Demir, Characterization of size-quantized PbTe thin films synthesized by an electrochemical co-deposition method, Thin Solid Films 517 (2009) 5419–5424.
[19] T. Oznuluer, I. Erdogan, I. Sisman, U. Demir, Electrochemical atom-by-atom growth of PbS by modified ECALE method, Chem. Mater. 17 (2005) 935–937.
[20] S. Ben Aoun, Z. Dursun, T. Sotomura, I. Taniguchi, Effect of metal ad-layers on Au (111) electrodes on electrocatalytic reduction of oxygen in an alkaline solution, Electrochem. Commun. 6 (2004) 747–752.
[21] M. Li, P. Liu, R.R. Adzic, Platinum monolayer electrocatalysts for anodic oxidation of alcohols, J. Phys. Chem. Lett. 3 (2012) 3480–3485.
[22] L.D. Zhu, T.S. Zhao, J.B. Xu, Z.X. Liang, Preparation and characterization of carbon-supported sub-monolayer palladium decorated gold nanoparticles for the electro-oxidation of ethanol in alkaline media, J. Power Sources 187 (2009) 80–84.
[23] Z. Dursun, S.U. Karabiberoglu, B. Gelmez, A. Basaran, Electrocatalytic oxidation of ethanol on various metal ad-layer modified Au(111) electrodes in alkaline solution, Turk. J. Chem. 35 (2011) 349–359.
[24] R. Reske, H. Mistry, F. Behafarid, B.R. Cuenya, P. Strasser, Particle size effects in the catalytic electroreduction of CO2 on Cu nanoparticles, J. Am. Chem. Soc. 136 (2014) 6978–6986.
[25] J. Luo, S.S. Jiang, H.Y. Zhang, J.Q. Jiang, X.Y. Liu, A novel non-enzymatic glucose sensor based on Cu nanoparticle modified graphene sheets electrode, Anal. Chim. Acta 709 (2012) 47–53.
[26] V. Singh, D. Joung, L. Zhai, S. Das, S.I. Khondaker, S. Seal, Graphene based materials: past, present and future, Prog. Mater. Sci. 56 (2011) 1178–1271.
[27] L. Karuppasamy, C.-Y. Chen, S. Anandan, J.J. Wu, Sonochemical fabrication of reduced graphene oxide supported Au nano dendrites for ethanol electrooxidation in alkaline medium, Catal. Today 307 (June (1)) (2018) 308–317.
[28] Q. Dong, Y. Zhao, X. Han, Y. Wang, M.C. Liu, Y. Li, Pd/Cu bimetallic nanoparticles supported on graphene nanosheets: facile synthesis and application as novel electrocatalyst for ethanol oxidation in alkaline media, Int. J. Hydrogen Energy 39 (2014) 14669–14679.
[29] X. Yang, Q.D. Yang, J. Xu, C.S. Lee, Bimetallic PtPd nanoparticles on Nafion-graphene film as catalyst for ethanol electro-oxidation (vol 22, pg 8057, 2012), J. Mater. Chem. 22 (2012) 25492.
[30] Y.T. Zhang, H.H. Shu, G. Chang, K. Ji, M. Oyama, X. Liu, Y.B. He, Facile synthesis of palladium-graphene nanocomposites and their catalysis for electro-oxidation of methanol and ethanol, Electrochim. Acta 109 (2013) 570–576.
[31] M.S. Ahmed, S. Jeon, Highly active graphene-supported NixPd100-x binary alloyed catalysts for electro-oxidation of ethanol in an alkaline media, ACS Catal. 4 (2014) 1830–1837.
[32] P. Mondal, A. Sinha, N. Salam, A.S. Roy, N.R. Jana, S.M. Islam, Enhanced catalytic performance by copper nanoparticle-graphene based composite, RSC Adv. 3 (2013) 5615–5623.
[33] S. Trasatti, O.A. Petrii, Real surface-area measurements in electrochemistry, J. Electroanal. Chem. 327 (1992) 353–376.
[34] E. Rouya, S. Cattarin, M.L. Reed, R.G. Kelly, G. Zangari, Electrochemical characterization of the surface Area of nanoporous gold films, J. Electrochem. Soc. 159 (2012) K97–K102.
[35] M.F. Toney, J.N. Howard, J. Richer, G.L. Borges, J.G. Gordon, O.R. Melroy, Electrochemical deposition of copper on a gold electrode in sulfuric-acid–resolution of the interfacial structure, Phys. Rev. Lett. 75 (1995) 4472–4475.
[36] M. Nishizawa, T. Sunagawa, H. Yoneyama, Underpotential deposition of copper on gold electrodes through self-assembled monolayers of propanethiol, Langmuir 13 (1997) 5215–5217.
[37] C. Kartal, Y. Hanedar, T. Oznuluer, U. Demir, Stoichiometry, morphology, and size-controlled electrochemical fabrication of CuxO (x = 1, 2) at underpotential, Langmuir 33 (2017) 3960–3967.
[38] D.M. Kolb, M. Przasnyski, H. Gerischer, Underpotential deposition of metals and work function differences, J. Electroanal. Chem. 54 (1974) 25–38.
[39] H. Gerischer, D.M. Kolb, M. Przasnyski, Chemisorption of metal atoms on metal-surfaces in correlation to work function differences, Surf. Sci. 43 (1974) 662–666.
[40] H.O. Dogan, D. Ekinci, U. Demir, Atomic scale imaging and spectroscopic characterization of electrochemically reduced graphene oxide, Surf. Sci. 611 (2013) 54–59.
[41] C.B. Liu, K. Wang, S.L. Luo, Y.H. Tang, L.Y. Chen, Direct electrodeposition of graphene enabling the one-step synthesis of graphene-metal nanocomposite films, Small 7 (2011) 1203–1206.
[42] L.Y. Chen, Y.H. Tang, K. Wang, C.B. Liu, S.L. Luo, Direct electrodeposition of reduced graphene oxide on glassy carbon electrode and its electrochemical application, Electrochem. Commun. 13 (2011) 133–137.
[43] J. Yang, S. Gunasekaran, Electrochemically reduced graphene oxide sheets for use in high performance supercapacitors, Carbon 51 (2013) 36–44.

[44] S.K. Bikkarolla, P. Cumpson, P. Joseph, P. Papakonstantinou, Oxygen reduction reaction by electrochemically reduced graphene oxide, Faraday Discuss. 173 (2014) 415–428.
[45] O.M. Magnussen, J. Hotlos, R.J. Nichols, D.M. Kolb, R.J. Behm, Atomic-Structure of Cu adlayers on Au(100) and Au(111) electrodes observed by insitu scanning tunneling microscopy, Phys. Rev. Lett. 64 (1990) 2929–2932.
[46] N. Batina, T. Will, D.M. Kolb, Study of the initial-stages of copper deposition by in-situ scanning-tunneling-microscopy, Faraday Discuss. 94 (1992) 93–106.
[47] Y. Yanson, J.W.M. Frenken, M.J. Rost, A general model of metal underpotential deposition in the presence of thiol-based additives based on an in situ STM study, Phys. Chem. Chem. Phys. 13 (2011) 16095–16103.
[48] C.S. Lai, X.X. Hu, S. Yau, W.P. Dow, Y.L. Lee, Electrodeposition of copper on an Au (111) electrode modified with mercaptoacetic acid in sulfuric acid, Electrochim. Acta 203 (2016) 272–280.
[49] B. Purusottam-Reddy, K. Sivajee-Ganesh, K. Jayanth-Babu, O.M. Hussain, C.M. Julien, Microstructure and supercapacitive properties of rf-sputtered copper oxide thin films: influence of O-2/Ar ratio, Ionics 21 (2015) 2319–2328.
[50] Z.H. Gan, G.Q. Yu, B.K. Tay, C.M. Tan, Z.W. Zhao, Y.Q. Fu, Preparation and characterization of copper oxide thin films deposited by filtered cathodic vacuum arc, J. Phys. D Appl. Phys. 37 (2004) 81–85.
[51] C.V. Niveditha, M.J.J. Fatima, S. Sindhu, Comprehensive interfacial study of potentio-dynamically synthesized copper oxide thin films for photoelectrochemical applications, J. Electrochem. Soc. 163 (2016) H426–H433.
[52] G.K. Ramesha, S. Sampath, Electrochemical reduction of oriented graphene oxide films: an in situ Raman spectroelectrochemical study, J. Phys. Chem. C 113 (2009) 7985–7989.
[53] A.C. Ferrari, J. Robertson, Interpretation of Raman spectra of disordered and amorphous carbon, Phys. Rev. B 61 (2000) 14095–14107.
[54] K.N. Kudin, B. Ozbas, H.C. Schniepp, R.K. Prud'homme, I.A. Aksay, R. Car, Raman spectra of graphite oxide and functionalized graphene sheets, Nano Lett. 8 (2008) 36–41.
[55] G.X. Wang, J. Yang, J. Park, X.L. Gou, B. Wang, H. Liu, J. Yao, Facile synthesis and characterization of graphene nanosheets, J. Phys. Chem. C 112 (2008) 8192–8195.
[56] A. Pendashteh, M.F. Mousavi, M.S. Rahmanifar, Fabrication of anchored copper oxide nanoparticles on graphene oxide nanosheets via an electrostatic coprecipitation and its application as supercapacitor, Electrochim. Acta 88 (2013) 347–357.
[57] M. Yin, C.K. Wu, Y.B. Lou, C. Burda, J.T. Koberstein, Y.M. Zhu, S. O'Brien, Copper oxide nanocrystals, J. Am. Chem. Soc. 127 (2005) 9506–9511.
[58] B.K. Park, S. Jeong, D. Kim, J. Moon, S. Lim, J.S. Kim, Synthesis and size control of monodisperse copper nanoparticles by polyol method, J. Colloid Interface Sci. 311 (2007) 417–424.
[59] S. Cherevko, N. Kulyk, C.H. Chung, Utilization of surface active sites on gold in preparation of highly reactive interfaces for alcohols electrooxidation in alkaline media, Electrochim. Acta 69 (2012) 190–196.
[60] R.K. Pandey, V. Lakshminarayanan, Ethanol electrocatalysis on gold and conducting polymer nanocomposites: a study of the kinetic parameters, Appl. Catal. B-Environ. 125 (2012) 271–281.
[61] R.K. Pandey, Y. Kawabata, S. Teraji, T. Norisuye, Q. Tran-Cong-Miyata, S. Soh, H. Nakanishi, Metal nanowire-based hybrid electrodes exhibiting high charge/discharge rates and long-lived electrocatalysis, ACS Appl. Mater. Interfaces 9 (2017) 36350–36357.
[62] Y. Kwon, S.C.S. Lai, P. Rodriguez, M.T.M. Koper, Electrocatalytic oxidation of alcohols on Gold in alkaline media: base or gold catalysis? J. Am. Chem. Soc. 133 (2011) 6914–6917.
[63] S.S. Mahapatra, A. Dutta, J. Datta, Temperature effect on the electrode kinetics of ethanol oxidation on Pd modified Pt electrodes and the estimation of intermediates formed in alkali medium, Electrochim. Acta 55 (2010) 9097–9104.
[64] Z. Qi, H.R. Geng, X.G. Wang, C.C. Zhao, H. Ji, C. Zhang, J.L. Xu, Z.H. Zhang, Novel nanocrystalline PdNi alloy catalyst for methanol and ethanol electro-oxidation in alkaline media, J. Power Sources 196 (2011) 5823–5828.
[65] D.A. Cantane, W.F. Ambrosio, M. Chatenet, F.H.B. Lima, Electro-oxidation of ethanol on Pt/C, Rh/C, and Pt/Rh/C-based electrocatalysts investigated by on-line DEMS, J. Electroanal. Chem. 681 (2012) 56–65.
[66] A.L. Wang, H. Xu, J.X. Feng, L.X. Ding, Y.X. Tong, G.R. Li, Design of Pd/PANI/Pd sandwich-structured nanotube array catalysts with special shape effects and synergistic effects for ethanol electrooxidation, J. Am. Chem. Soc. 135 (2013) 10703–10709.
[67] R.B. de Lima, H. Varela, Catalytic oxidation of ethanol on gold electrode in alkaline media, Gold Bull. 41 (2008) 15–22.
[68] Q.Y. Wang, X.Q. Cui, W.M. Guan, X.M. Zhang, C. Liu, T.Y. Xue, H.T. Wang, W.T. Zheng, A nanoflower shaped gold-palladium alloy on graphene oxide nanosheets with exceptional activity for electrochemical oxidation of ethanol, Microchim. Acta 181 (2014) 373–380.
[69] L. Zhang, H. Wang, X.C. Li, F.L. Xia, Y. Liu, X.Y. Xu, J.P. Gao, F.B. Xing, One-step synthesis of palladium-gold-silver ternary nanoparticles supported on reduced graphene oxide for the electrooxidation of methanol and ethanol, Electrochim. Acta 172 (2015) 42–51.
[70] P. Mukherjee, P.S. Roy, K. Mandal, D. Bhattacharjee, S. Dasgupta, S.K. Bhattacharya, Improved catalysis of room temperature synthesized Pd-Cu alloy nanoparticles for anodic oxidation of ethanol in alkaline media, Electrochim. Acta 154 (2015) 447–455.
[71] C. Bianchini, P.K. Shen, Palladium-based electrocatalysts for alcohol oxidation in half cells and in direct alcohol fuel cells, Chem. Rev. 109 (2009) 4183–4206.
[72] Z.Y. Zhou, Q.A. Wang, J.L. Lin, N. Tian, S.G. Sun, In situ FTIR spectroscopic studies of electrooxidation of ethanol on Pd electrode in alkaline media, Electrochim. Acta 55 (2010) 7995–7999.
[73] W.X. Du, K.E. Mackenzie, D.F. Milano, N.A. Deskins, D. Su, X.W. Teng, Palladium-Tin alloyed catalysts for the ethanol oxidation reaction in an alkaline medium, ACS Catal. 2 (2012) 287–297.
[74] W.G. Pell, B.E. Conway, W.A. Adams, J. de Oliveira, Electrochemical efficiency in multiple discharge recharge cycling of supercapacitors in hybrid EV applications, J. Power Sources 80 (1999) 134–141.
[75] M. Wang, Z.Z. Ma, R.X. Li, B. Tang, X.Q. Bao, Z.H. Zhang, X.G. Wang, Novel flower-like PdAu(Cu) anchoring on a 3D rGO-CNT sandwich-stacked framework for highly efficient methanol and ethanol electro-oxidation, Electrochim. Acta 227 (2017) 330–344.
[76] X.-Z. Yuan, C. Song, H. Wang, J. Zhang, EIS Equivalent Circuits, Springer, 2010.
[77] C.Q. Wang, H.W. Wang, C.Y. Zhai, F.F. Ren, M.S. Zhu, P. Yang, Y.K. Du, Three-dimensional Au-0.5/reduced graphene oxide/Au-0.5/reduced graphene oxide/carbon fiber electrode and its high catalytic performance toward ethanol electro-oxidation in alkaline media, J. Mater. Chem. A 3 (2015) 4389–4398.
[78] J.L. Zhang, M.B. Vukmirovic, K. Sasaki, A.U. Nilekar, M. Mavrikakis, R.R. Adzic, Mixed-metal Pt monolayer electrocatalysts for enhanced oxygen reduction kinetics, J. Am. Chem. Soc. 127 (2005) 12480–12481.
[79] J. Zhang, Y. Mo, M.B. Vukmirovic, R. Klie, K. Sasaki, R.R. Adzic, Platinum monolayer electrocatalysts for O-2 reduction: Pt monolayer on Pd(111) and on carbon-supported Pd nanoparticles, J. Phys. Chem. B 108 (2004) 10955–10964.
[80] X.L. Zhang, Z.S. Lu, Z.X. Yang, A comparison study of oxygen reduction on the supported Pt, Pd, Au monolayer on WC(0001), J. Power Sources 321 (2016) 163–173.